

Vanadium-Doped Monolayer MoS₂ with Tunable Optical Properties for Field-Effect Transistors

Jian Zhang, Yi Zhu, Mike Tebyetekerwa, Delong Li, Dan Liu, Weiwei Lei,* Lifeng Wang,* Yupeng Zhang,* and Yuerui Lu*



Cite This: *ACS Appl. Nano Mater.* 2021, 4, 769–777



Read Online

ACCESS |



Metrics & More



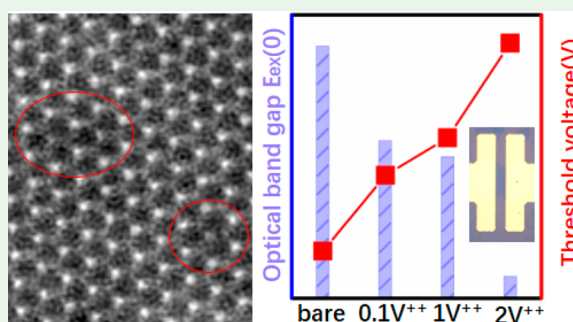
Article Recommendations



Supporting Information

ABSTRACT: Substitutional doping is a promising methodology to tune the optoelectronic properties of transition metal dichalcogenides (TMDs). However, to this date, direct substitution of transition metal atoms in monolayer regime has only been demonstrated with few metal atoms. Herein monolayer (ML) molybdenum disulfide (MoS₂) doped with different concentrations of vanadium(V) is successfully prepared by tuning the molar ratio of MoO₃ and V₂O₅ powder in a chemical vapor deposition (CVD) process. Interestingly, photoluminescence (PL) intensity of the V-doped ML MoS₂ with optimal ratio is four times larger than that of intrinsic MoS₂. Further PL spectra fittings indicate that the exciton recombination in V-doped samples is dominant relative to the trion recombination due to the p-doping effect, which is further confirmed by the gate-dependent PL testing. It is also observed that the optical bandgap of MoS₂ and the threshold voltage of as-fabricated field-effect transistors (FETs) can be tuned through controllable V doping. As a proof of concept, ML MoSe₂ doped with V also exhibits enhanced PL intensity due to the p-doping effect. The successful preparation of Mo-based monolayer TMDs with controllable vanadium doping could be helpful for optical absorption-based optoelectronic applications.

KEYWORDS: substitutional doping, doping level, exciton recombination, p-doping effect, tunable optical band gap



1. INTRODUCTION

Because of their unique electronic and optical properties, layered transition metal dichalcogenides (TMDs) have shown great potential in two-dimensional electronic, optoelectronic, and spintronic devices.^{1–4} Especially, due to thickness-dependent energy band structure⁵ and extremely large coulomb interaction-induced stable exciton states in monolayer form, molybdenum disulfide (MoS₂) was widely studied for optoelectronic-related applications. However, monolayer (ML) MoS₂ always shows a relatively lower PL intensity due to the existence of sulfur vacancies.⁶ In this regard, several approaches including electrostatic gating,⁷ chemical treatment,^{8,9} laser irradiation,^{10–12} and chemical doping¹³ have been adopted to improve the optoelectronic properties of ML MoS₂. Among these methods, chemical doping was believed to be an efficient and facile method to modify the carrier density of ML MoS₂. For instance, p-type F₄-TCNQ and n-type NADH dopants were used to tune the PL intensities of ML MoS₂, and the PL intensity was largely enhanced by doping with p-type dopants but was significantly decreased by doping with n-type dopants, attributed to surface charge transfer between dopants and ML MoS₂.¹⁴ Furthermore, ML MoS₂ modified with various types of molecules, such as potassium,¹⁵ benzyl viologen,¹⁶ cesium carbonate,¹⁷ chloride molecules,¹⁸ etc., were also reported for the enhancement of optoelectronic

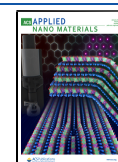
properties through surface charge transfer. However, the related surface charge transfer dopants can easily escape from the surface of MoS₂ after vacuum pumping or thermal annealing, leading to device instability in optoelectronic applications.

Different from surface charge transfer doping, substitutional dopants in the MoS₂ honeycomb network could be more applicable for device application due to the formation of chemical bonds between doping elements and Mo or S atoms. Moreover, several theoretical ab initio studies^{19–22} have predicted the effects of metal-site substitutional dopants on structural, electrical, phonon, magnetic, and optical properties of TMDs, further indicating the important role of substitutional doping. But so far, experimental reports of direct substitution of transition metal atoms^{23–25} in the monolayer form are still scarce. Recently, Mn-doped MoS₂ was successfully prepared via CVD, and the band structure of MoS₂ was also modulated by incorporation of Mn. Moreover,

Received: November 19, 2020

Accepted: December 7, 2020

Published: December 31, 2020



the authors demonstrated that the suitable selection of substrate plays a vital role in Mn doping. The inert substrate is feasible for the incorporation of a large number of Mn atoms in MoS₂, while the commonly used substrate, such as SiO₂ and sapphire, prevents the injection of Mn, which may limit its application in optoelectrical areas.²⁶ In another study, atomically thin WS₂ and MoS₂ monolayers doped with niobium (Nb) and rhenium (Re) also exhibited direct-gap semiconductor behavior. Moreover, combining first-principles calculations with related experimental results, the electronic structure of Re-doped MoS₂ was also detailed, and it was found that Re doping enables ohmic contact between the metal and MoS₂, making it useful for such doped TMDs in optoelectronics devices.²⁷ However, current work on substitutional doping usually lacks the tuning of doping concentration, which can lead to imperfection and even the degeneration of related optoelectronic properties. Therefore, developing a facile, scalable, and controllable substitutional doping methodology is still challenging and necessary for future optoelectronic applications.

In this work, V-doped MoS₂ with a series of doping concentrations was successfully prepared during the CVD growth of monolayer MoS₂ for the investigation of the doping effect and the optimization of optoelectronic properties. Together with Raman spectroscopy and atomic force microscopy (AFM), X-ray photoelectron spectroscopy (XPS) and transmission electron microscopy (TEM) mapping indicate the substitutional doping of V in monolayer MoS₂. The V-doped MoS₂ exhibits dramatically enhanced PL intensity relative to bare MoS₂, while a further increase in doping concentration leads to slightly decreased PL intensity because an excess of V atoms can set a nonrecombination center. It was also found that the ratio of trion to total PL intensity decreases with increasing doping concentration, which was attributed to the p-doping effect, making the dominant PL process change from negative trion recombination to exciton recombination. The similar trend of trion intensity in gate-dependent PL of V-doped MoS₂ confirms the p-doping effect of V doping. Additionally, a single flake of as-prepared monolayer samples was utilized to construct field-effect transistor (FET) devices, and the threshold voltage of V-doped samples shifts toward positive voltage with increasing doping concentration, further indicating the p-doping effect of substitutional V doping. Moreover, according to low-temperature PL fitting results, we found that the optical band gap of MoS₂ can also be modulated by substitutional V doping, which can be further used for optical absorption-related applications. Together with the effect of V doping on optical properties of monolayer MoSe₂, our results provide the fundamental understanding of how V doping of two-dimensional layers affects the optical properties and the corresponding electrical properties, enabling the realization of TMD with tunable optoelectronic properties and potential magnetic properties.

2. EXPERIMENTAL SECTION

2.1. CVD Growth of Bare Monolayer MoS₂ and V-Doped MoS₂. MoS₂ and V-doped MoS₂ crystals were grown on SiO₂/Si dielectric substrate by using ambient pressure chemical vapor deposition. MoO₃ powder and V₂O₅ powder with different weight ratios (8/0, 8/0.1, 8/1, and 8/2) were put into the center zone of a horizontal furnace. A 100 mg amount of sulfur powder was placed at the center of another horizontal furnace. SiO₂/Si substrates were cleaned with acetone/2-propanol/water and placed face down just above the MoO₃ powder and V₂O₅ powder to ensure maximum

exposure of MoO₃ and V₂O₅ vapor to the substrate surface. Using Ar/H₂ mixed gases as carrier gas, the furnace temperature was raised to 750 °C and 300 °C at a rate of 10 °C/min, respectively. After stabilization of the system for 15 min, the furnace was cooled to room temperature. In this work, bare MoS₂ and V-doped MoS₂ with different doping concentrations were denoted as bare MoS₂, 0.1 V-MoS₂, 1 V-MoS₂, and 2 V-MoS₂, respectively. Here the number in front of marked samples stands for the nominal doping concentration. Additionally, bare MoSe₂ and V-doped MoSe₂ were also prepared by instead using Se powder, and the weight ratio of MoO₃ and V₂O₅ was 8:1.

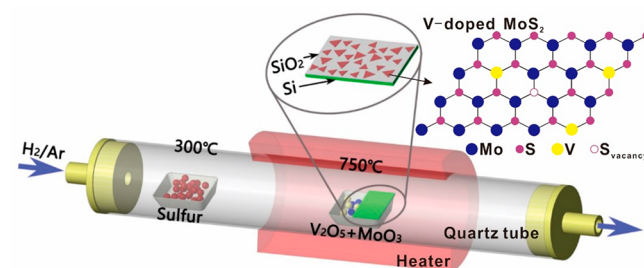
2.2. Device Fabrication and Measurement. The back-gate FET devices were fabricated by using photolithography techniques. The specific parameters for photolithography can be found in our previous work, including the selection of photoresist, spin or baking processing parameters, UV exposure time and the following electron-beam deposition, and electrical measurement conditions.

2.3. Material Characterization. The as-prepared bare MoS₂ and V-doped MoS₂ with different doping concentrations were characterized by optical microscopy. AFM and Raman spectroscopy were employed to identify the phase structure and the layer number. The chemical state was examined by XPS that was also used in our previous work²⁸ (binding energy refers to C 1s peak at 284.9 eV). A 300-mesh Cu grid with porous carbon film was used for TEM mapping tests, and the sample was transferred by a PMMA (poly(methyl methacrylate))-assisted wetting transfer method. The detailed information about the optical path length (OPL), PL, and Raman testing equipment (light source, diameter of illuminated spot) can also be found in our previous work.²⁸ Here it is worth noting that the on-sample excitation power for bare MoS₂ and V-doped MoS₂ was always 200 μW, and the acquisition time was 5 s for the room-temperature and low temperature PL measurements, whereas the acquisition time for PL spatial mapping was 1 s. While the sample excitation power for bare ML MoSe₂ and V-doped ML MoSe₂ is always 50 μW, the acquisition times is 1 s for room-temperature PL measurements and PL spatial mapping. Concerning temperature-dependent PL measurements, the samples were placed into a microscopy-compatible chamber with a low-temperature controller (using liquid nitrogen as the coolant). For the gate-dependent PL measurements, the related fabricating and testing process can also be found in our previous work.²⁸

3. RESULTS AND DISCUSSION

The large-area monolayer MoS₂ and V-doped MoS₂ were directly grown on a 280 nm SiO₂/Si substrate by the vapor-phase reaction of MoO₃ with different V concentrations and sulfur powders in a hot-wall CVD system. Scheme 1 illustrates

Scheme 1. CVD Growth Process of V-Doped MoS₂



the furnace setup, sulfur powders are located upstream of the hot zone, and V₂O₅ mixed with MoO₃ with different ratios are located in the hot zone during synthesis. Figure S1 shows the optical micrograph of bare MoS₂ and V-doped MoS₂ synthesized on SiO₂/Si substrates, exhibiting a triangular shape with the lateral size up to 10–20 μm. Herein bare MoS₂

and V-doped MoS₂ with different doping concentrations are denoted as bare MoS₂, 0.1 V-MoS₂, 1 V-MoS₂, and 2 V-MoS₂, respectively. For bare MoS₂, the Raman spectra (Figure 1a)

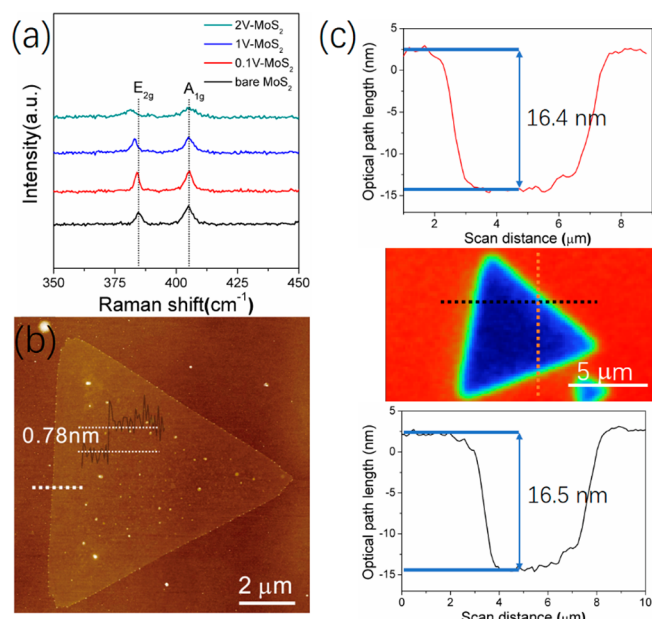


Figure 1. (a) Raman spectra of bare MoS₂ and V-doped MoS₂ with different doping concentrations. (b) AFM image of 0.1 V-MoS₂ and (c) phase-shifting interferometry (PSI) measured optical path length (OPL) values of 0.1 V-MoS₂ along the dashed line.

show typical vibration modes (A_{1g} and E_{2g}) of MoS₂ at 404.9 and 384.5 cm^{-1} , with a 20.4 cm^{-1} difference between A_{1g} and E_{2g} , indicating the monolayer characteristic of MoS₂.²⁹ It can also be found that the frequency of the in-plane vibration mode (E_{2g} peak) is red-shifted gradually with increasing doping concentration, while the frequency of the A_{1g} peak (out-of-plane) is almost unaffected and the intensity of A_{1g} decreased after V doping. It should be noted that the commonly reported red-shift of A_{1g} after doping was due to the increased electron concentration that increases the electron–phonon scattering.^{24,30} However, the decreased A_{1g} peak intensity and unaffected A_{1g} frequency could be attributed to the decreased electron concentration, probably indicating the p-doping effect of V incorporation.³¹ Because E_{2g} represents the in-plane vibration of molybdenum and sulfur atoms, the red-shift of E_{2g} in this work possibly arises from the incorporation of V atoms into the MoS₂ lattice. The AFM image in Figure 1b indicates ~ 0.78 nm thickness of the as-prepared sample, revealing the monolayer characteristic of 0.1 V-MoS₂. In our previous work, phase-shifting interferometry (PSI) was confirmed to be a reliable way to determine the layer number of two-dimensional materials,^{32–34} depending on the contrast under optical microscopy. Therefore, the monolayer characteristics of 0.1 V-MoS₂ were further identified by the contrast under optical microscopy. The OPLs of the horizontal and vertical lines across the nanosheet in 0.1 V-MoS₂ are 16.5 and 16.4 nm (Figure 1c), which can be a criterion to determine the layer number of bare MoS₂ and the other doped samples. Here PSI was also used to confirm the layer number of bare MoS₂, 1 V-MoS₂, and 2 V-MoS₂ (Figure S2), and the corresponding

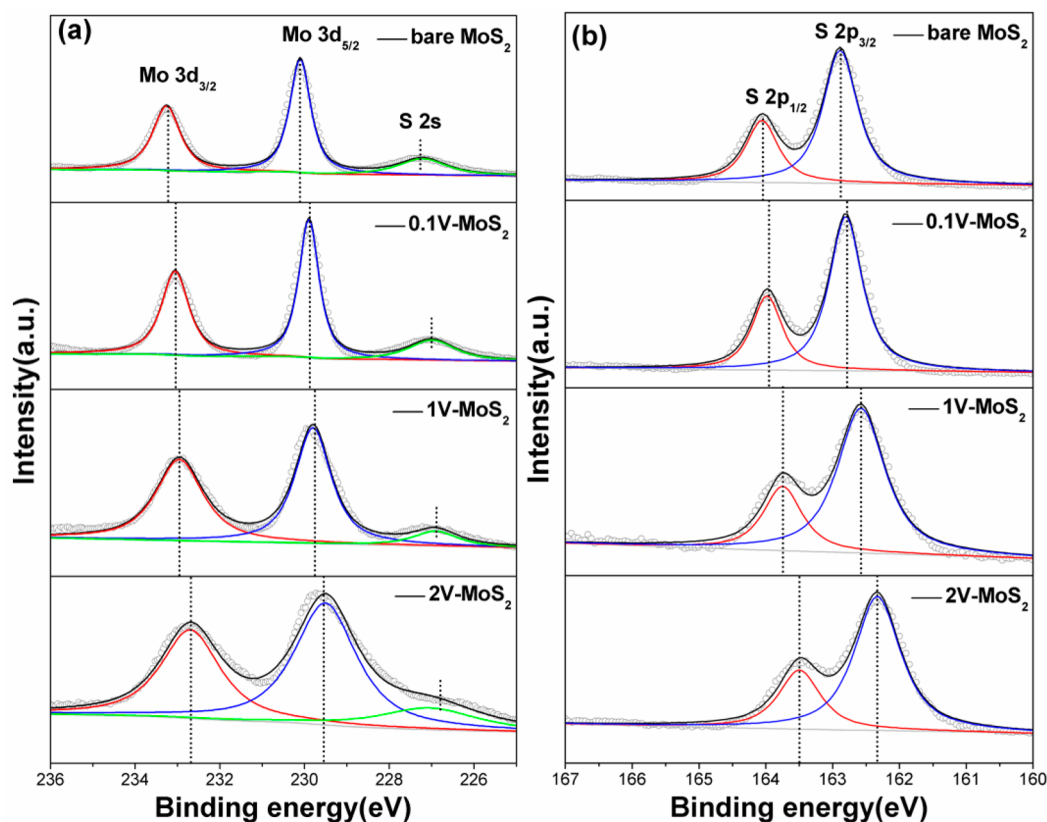


Figure 2. (a) Mo 3d and (b) S 2p spectra of V-doped MoS₂ with different concentrations.

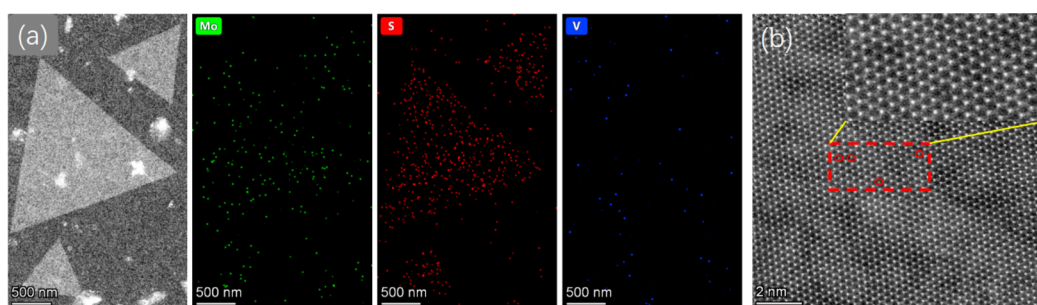


Figure 3. (a) TEM image and the corresponding elemental mapping results of 2 V-MoS₂. (b) Atomic resolution STEM-ADF image of 2 V-MoS₂; inset shows the magnified image based on the red rectangular region.

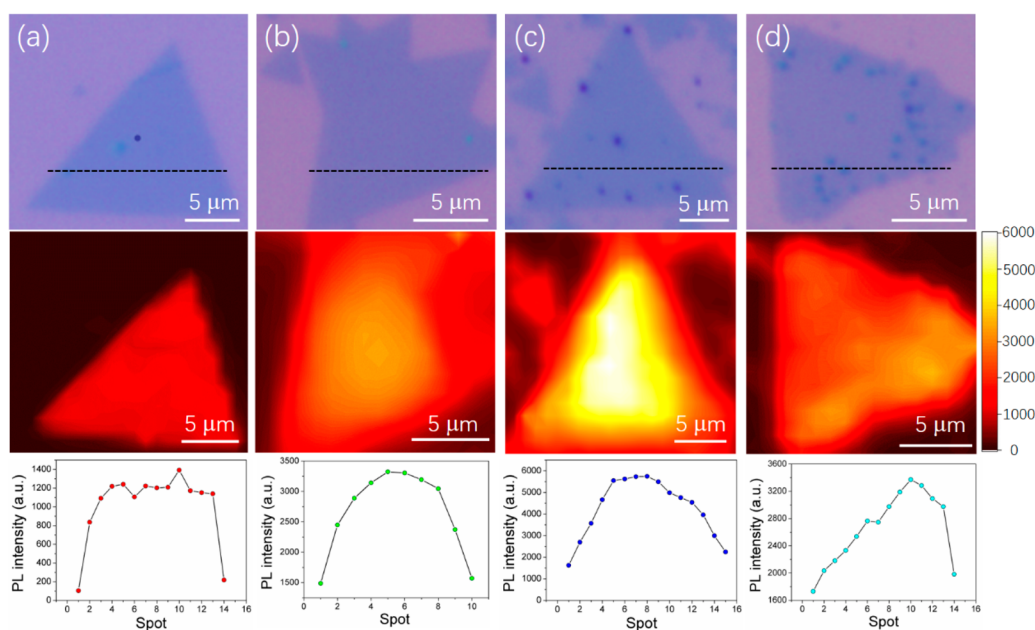


Figure 4. Optical image, the corresponding PL intensity mapping, and extracted PL intensity along the dotted line of bare MoS₂ (a), 0.1 V-MoS₂ (b), 1 V-MoS₂ (c), and 2 V-MoS₂ (d).

OPLs are almost equal to that of 0.1 V-MoS₂, indicating the monolayer characteristic of the as-prepared samples.

To further illustrate the effect of V doping on the chemical structure and energy levels of MoS₂, XPS spectra of V-doped MoS₂, with different doping concentrations, as well as bare MoS₂ are carried out. Figure 2(a,b) shows that the Mo 3d and S 2p peaks of V-doped samples gradually shift to lower binding energy with increasing doping concentration compared to bare MoS₂, indicating that the Fermi level of V-doped MoS₂ shifts closer to the valence band. The lowering of the Fermi level of V-doped samples indicates that V introduces p-type doping in the MoS₂ monolayer.²³ According to the survey spectra of as-prepared samples (Figure S3), the Mo, S, O, and C elements are characterized. However, the V element cannot be detected, possibly due to the tiny amount of V element relative to the main Mo and S elements. Here, to further probe the composition and spatial distribution of the constituent elements in as-prepared doped samples, energy-dispersive X-ray (EDX) spectroscopy under scanning transmission electron microscopy (STEM) was carried out based on 2 V-MoS₂, as shown in Figure 3a. The element mapping results indicate the existence of V element. Additionally, the STEM-ADF (annular dark field) image of 2 V-MoS₂ is also given in Figure 3b. Due to differences in atomic Z-numbers, V atoms should display a

darker contrast compared to that of Mo atoms.³⁵ According to the inserted magnified image in Figure 3b, V atoms with a darker contrast occupy the Mo sites, corresponding to the area with red circles. Therefore, together with the binding energy shift and the lowered Fermi level of V-doped samples in the XPS spectra, it can be concluded that V as a kind of doping element was indeed incorporated into the MoS₂ lattice.

It is well-known that CVD-grown TMDs usually exhibit different PL intensities at the edge and core of nanosheets. To clearly investigate the effect of V doping on the luminescent properties of monolayer MoS₂, the optical images and the corresponding room-temperature PL intensity spatial mapping for bare MoS₂, 0.1 V-MoS₂, 1 V-MoS₂, and 2 V-MoS₂ are given in Figure 4(a–d). Obviously, bare MoS₂ shows weak PL intensity, possibly attributed to the large number of electrons induced by sulfur vacancies that transform most of the excitons into negative trions. On the contrary, according to the PL intensity mapping images of the as-prepared samples, the doped samples with different doping concentrations exhibit dramatically enhanced PL intensity. To further detail the PL intensity distribution of the as-prepared samples, the PL intensity along the dotted line was also extracted. It was found that the PL intensity of 1 V-MoS₂ in the central spot is nearly four times larger than that of bare MoS₂, and this enhancement

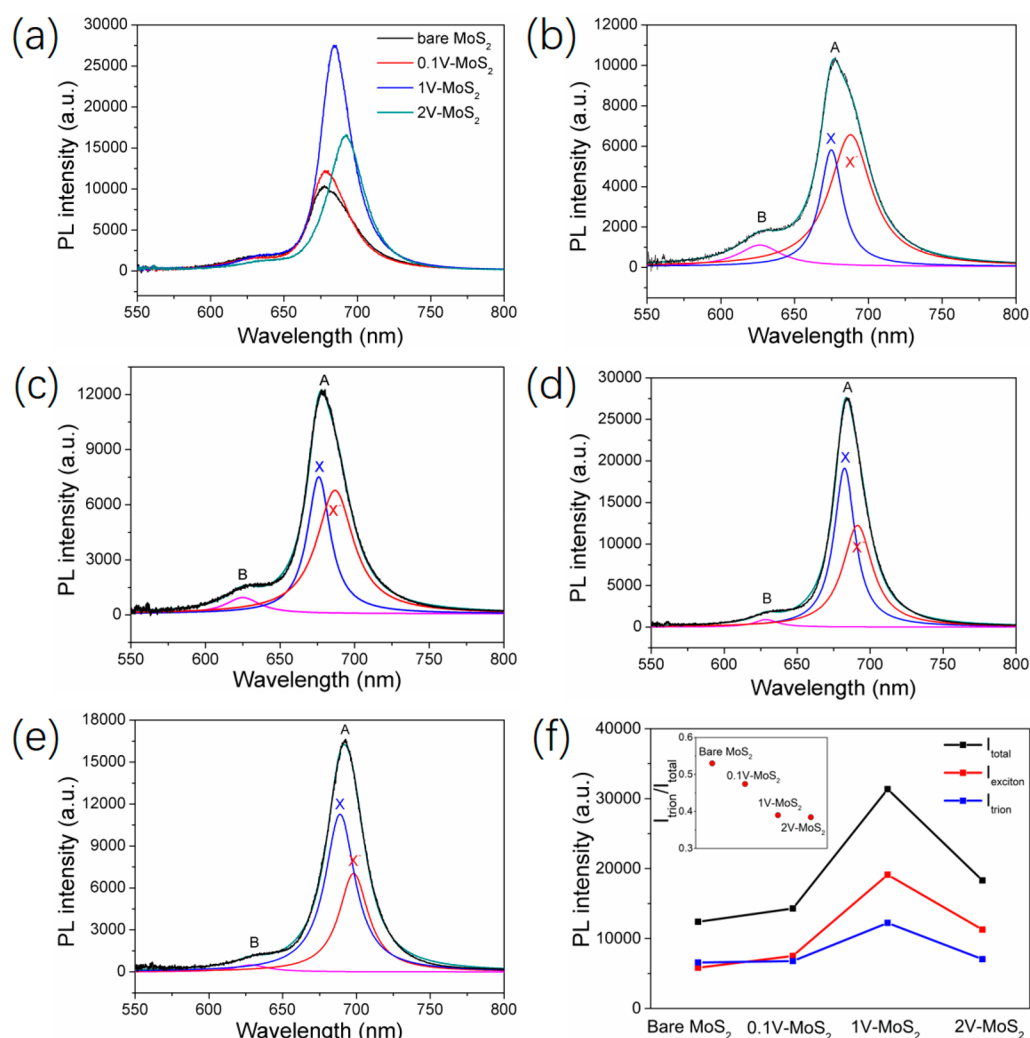


Figure 5. (a) PL spectra of the as-prepared samples, and the corresponding fitting curves of (b) bare MoS₂, (c) 0.1 V-MoS₂, (d) 1 V-MoS₂, and (e) 2 V-MoS₂. (f) The comparison of trion, exciton, and total intensity of the as-prepared samples. The inset shows the ratio of trion to total intensity in different samples.

is almost unaffected by excitation power, as shown in Figure S4. Because DFT (density functional theory) simulations³⁶ showed that the n-doping effect was achieved when the doping elements have more d-level electrons than those of Mo, otherwise exhibiting a p-doping effect,³⁷ there is a reason to believe that enhanced PL intensity of V-doped MoS₂ is attributed to the p-doping effect, which makes the dominant PL process change from negative trion recombination to exciton recombination. It should be noted that PL intensity of 2 V-MoS₂ decreased a little compared to 1 V-MoS₂. The main reason is that an excess of V atoms can serve as nonradiative recombination centers and then quench luminescence. Considering the differences between monolayer nanosheets in each sample, the PL intensity spatial mapping for these four samples based on the other monolayers was also tested, as shown in Figure S5. It was found that V-doped MoS₂ exhibited nonuniform PL intensity, possibly due to heterogeneous V doping. Despite this, the variation trend of PL intensity was consistent with the former results, indicating the reliability of the PL testing results.

For better comparison, further PL analyses are all based on PL spectra that are obtained from the center spot of monolayer MoS₂ with and without V doping. As shown in Figure 5a, the

peak position in PL spectra of monolayer MoS₂ is red-shifted with increasing doping concentration, and the changes in PL intensities of the as-prepared samples are consistent with the former spatial mapping results. Moreover, it can be found that V-doped MoS₂ exhibited line width narrowing compared to bare MoS₂, possibly attributed to the reduction of defect-related nonradiative recombination paths and suppression of the structural defects. To further understand the spectral changes of different samples, the spectral changes of the exciton (X) and the trion (X⁻) in peak A are considered. Peak A can be decomposed into the exciton peak and negative trion peak under the same Lorentzian fitting condition (adjacent R-square value equal to 0.9999). It was found that the PL spectral weight of the negative trion peak at 1.80 eV (red line) is greater than that of the exciton peak at 1.84 eV (blue line) in bare MoS₂ (Figure 5b). This experiment is in accordance with the formerly reported results,¹⁴ in which the trion recombination is dominant in as-prepared monolayer MoS₂ due to the unintentional electron doping. On the contrary, the PL spectra of monolayer MoS₂ after V doping are dominated by the exciton peak (Figure 5c–e), which confirms that the excitons can recombine without transforming to trions due to the decrease in the number of electrons in V-doped MoS₂,

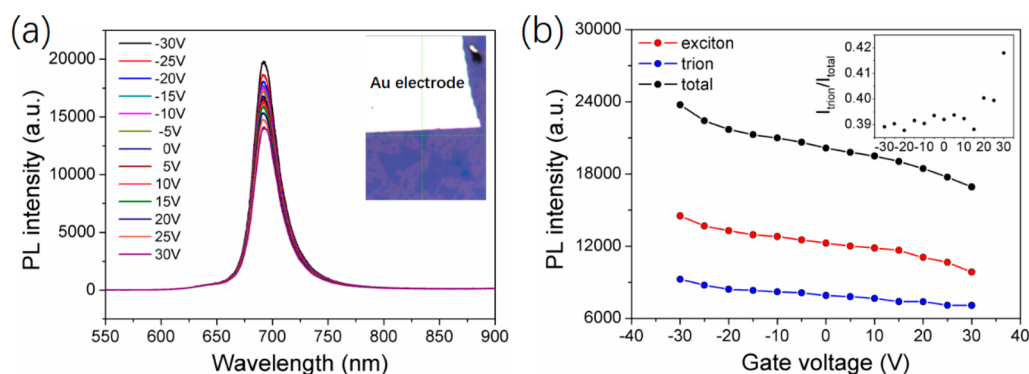


Figure 6. (a) Gate-dependent PL of 2 V-MoS₂. The inset shows the fabricated chip based on a triangular sample partly covered by the Au electrode for gate-dependent testing. (b) Comparison of trion and exciton intensity after fitting. The inset shows the ratio of trion intensity to total intensity under different gate voltages from -30 to 30 V.

indicating the p-doping effect of V-doped MoS₂. Figure 5f shows the integrated exciton and trion intensities as a function of the doping concentration. The integrated exciton intensity first increases with increasing doping concentration, but further increase in doping concentration (2 V-MoS₂) leads to degenerated exciton intensity. PL intensity is determined by the ratio of radiative and nonradiative recombination rates. Commonly, the nonradiative recombination rate contains the rates of defect trapping. With a further increase in V dopant, an excess of V atoms can be set as a defect state that exhibits an enhanced nonradiative recombination rate, leading to the decreased PL intensity of 2 V-MoS₂. According to Figure 5f, the ratio of trion intensity to total PL intensity for bare MoS₂, 0.1 V-MoS₂, 1 V-MoS₂, and 2 V-MoS₂ is 53.0%, 47.4%, 39.0%, and 38.4%, respectively. Similarly, considering the differences between nanosheets in each sample, the trion ratio of these four samples was calculated again based on the PL spectra extracted from Figure S5. On the basis of the extracted spectra in Figure S6a, the trion ratio of bare MoS₂, 0.1 V-MoS₂, 1 V-MoS₂, and 2 V-MoS₂ is calculated as 57.6%, 43.5%, 39.8%, and 39.2% (insert of Figure S6b), which also exhibits a monotonically decreased relative trion intensity with an increased V doping concentration. Additionally, together with the former two sets of data, a new set of data obtained from the other nanosheets of as-prepared samples is added, and the error bars are also calculated, as shown in Figure S7, revealing a similar decreased trion ratio with increased V dopant. Therefore, it is anticipated that V-doping induced hole injection neutralizes the electrons in monolayer MoS₂, making the exciton recombination prior to the negatively charged trion recombination.

It is also believed that the intensities of trions and neutral excitons can be modulated by applying gate voltage. Here, to confirm the effect of V doping on the optical properties of MoS₂, we also investigated the gate-dependent PL of doped samples. The device structure and the corresponding PL spectra are shown in Figure 6a. It should be pointed out that the as-prepared monolayer sample is grounded through the Au contact pad, and the n⁺-doped Si substrate functions as a back gate. Taking 2 V-MoS₂ as an example, the PL intensity was increased when applying negative voltage and was decreased under positive voltage. This phenomenon can be attributed to the interaction of excitons with gate-voltage-induced changes of free charge carriers in 2 V-MoS₂. Considering the largely increased PL intensity of V-doped samples, as described in Figure 4 and Figure 5a, the V-doping effect is equivalent to the

effect of imposed negative voltage, which injects the hole to neutralize the sulfur vacancy-induced electrons in MoS₂ and then improves the ratio of exciton recombination. Figure 6b presents the integrated exciton and trion intensities and their total contribution as a function of gate voltage for 2 V-MoS₂. It was also found that both exciton and trion intensity show a monotonous decrease with the change of gate voltage from -30 to 30 V. Different from commonly reported non-monotonous changes in exciton intensity and trion intensity,³⁸ the monotonous decreased intensity probably arise from the larger number of electrons that cannot be completely neutralized in the current negative voltage and cannot form positive charged trions. Moreover, according to the inset of Figure 6b, the ratio of trion to total intensity almost exhibits the monotonically decreased relative trion intensity with the gate voltage change from 30 to -30 V, which exhibits a similar change trend as in the inset of Figure 5f and Figure S6b, indicating the p-doping effect of V doping. It should be noted here that the tiny changes in PL intensity under the gate voltage could be attributed to the lower electron/hole injection efficiency of the as-prepared devices. Moreover, to further detail the effect of V doping on the optical properties of MoS₂, the FET properties of bare MoS₂ and V-doped MoS₂ with different doping concentrations were also measured. Figure S8 shows the $I_{ds}-V_g$ curves of the as-prepared samples at $V_{ds} = 0.5$ V. It was found that the bare monolayer MoS₂ exhibits an n-type semiconductor behavior with a threshold voltage at -10 V. After the V-doping process, the threshold voltage (V_{th}) is shifted in the positive direction from -10 to 12 V, while retaining a similar on/off ratio and obvious n-type behavior. Because the doped samples have electron density much lower than that of bare MoS₂, high positive V_g was needed to increase the electron concentration in FET channels, leading to a more positive threshold voltage in V-doped samples. The positive shift in threshold voltage further indicates the p-doping effect of V doping,³⁷ which is consistent with the former discussion.

Commonly, the PL peak energy of direct-bandgap semiconductors is equal to the optical bandgap.³⁹ Here, to further detail the effect of V doping on the PL peak energy and the corresponding optical bandgap of monolayer MoS₂, the temperature-dependent PL spectra of bare MoS₂, 0.1 V-MoS₂, 1 V-MoS₂, and 2 V-MoS₂ were also employed, as shown in Figure S9. The temperature-dependent PL spectra of the as-prepared samples all exhibit a blue-shift with decreasing temperature, which is consistent with the commonly reported band gap reduction with temperature for many semi-

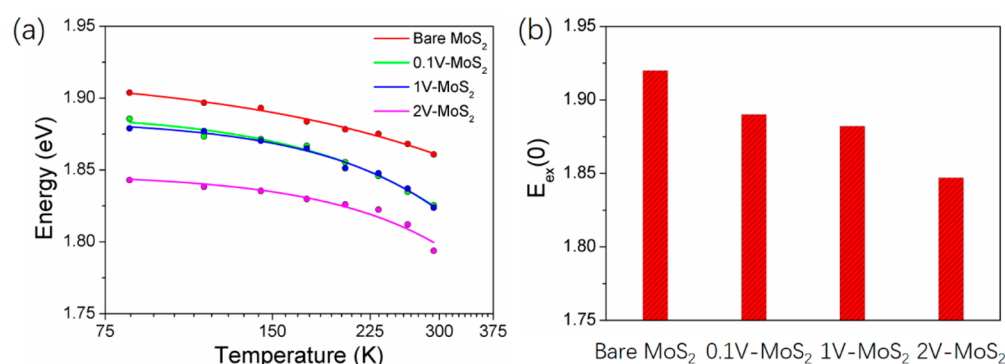


Figure 7. (a) Exciton peak position as a function of temperature for bare monolayer MoS₂, 0.1 V-MoS₂, 1 V-MoS₂, and 2 V-MoS₂. Dots stand for the raw data, and solid lines stand for the fitted curves. (b) Comparison of band gap values as T approaches 0 K.

conductors.⁸ Moreover, the temperature dependence of exciton and trion peak position and peak intensity in the as-prepared samples can also be extracted by using the same fitting method as described in Figure 5(b–e), as shown in Figure 7a. We find that the exciton peak position fits very well using a standard semiconductor bandgap dependence of $E_g(T) = E_g(0) - (\alpha T^2 / (T + \beta))$, where parameters α and β are constants, and $E_g(0)$ is the optical band gap value as T approaches 0 K.^{46,41} From further fits based on the former equation, the $E_g(0)$ for bare monolayer MoS₂, 0.1 V-MoS₂, 1 V-MoS₂, and 2 V-MoS₂ is 1.920, 1.890, 1.885, and 1.847 eV, respectively. Therefore, the red-shift in PL spectra of monolayer MoS₂ after V doping can be well explained by the gradually decreased optical bandgap of MoS₂ with increasing doping concentration (Figure 7b). The optical band gap usually describes the energy required to create an exciton (electron–hole pair) via optical absorption,⁴² which is usually dependent on the strain,⁴³ dielectric screening,⁴⁴ or alloying effect.⁴⁵ In this work, the alloying, substrate, and strain effect can be excluded by the nonexistent VSe₂ phase in the Raman spectra of doped samples and the similar synthesis conditions compared to bare MoS₂. A possible explanation for the decreased optical bandgap may be the doping effects acting on electron–hole interactions in V-doped samples with different exciton binding energies or electronic bandgaps. Additionally, the α values of bare MoS₂, 0.1 V-MoS₂, 1 V-MoS₂, and 2 V-MoS₂ are 3.8–4E eV/K, 5.2–4E eV/K, 4.4–4E eV/K, and 3.8–4E eV/K, respectively, and the β values of bare MoS₂, 0.1 V-MoS₂, 1 V-MoS₂, and 2 V-MoS₂ are 400 K, 400 K, 380 K, and 360 K, respectively. It was found that these two values are nearly the same among different samples with different doping concentrations, which are consistent with the reported α and β values.

As a proof of concept, V-doped MoSe₂ was also prepared by CVD. It was found that bare MoSe₂ and V-doped MoSe₂ both exhibited a triangular shape with a lateral size up to 10–20 μm , and the monolayer characteristics of the as-prepared samples were also confirmed by PSI testing (Figure S10), PL spectra, and Raman spectra (Figure S11). PL spatial mapping results revealed that the PL intensity of MoSe₂ after V doping was enhanced compared to bare MoSe₂, as shown in Figure S11. As an n-type semiconductor, the enhanced PL emission of V-doped MoSe₂ could be attributed to the decreased electron concentration in monolayer MoSe₂ after V doping, which is consistent with that of V-doped MoS₂, indicating the p-doping effect of V doping.

4. CONCLUSION

In summary, substitutional doping of vanadium(V) atoms with a series of doping concentrations was prepared by tuning the molar ratio of MoO₃ and V₂O₅ powder during the CVD process, and the tunable optical properties were also achieved. Compared to bare monolayer MoS₂, PL intensities of V-doped MoS₂ are dramatically enhanced with increasing doping concentration, and a further increase in V doping leads to a small decrease in PL intensity. Especially, the PL intensity of V-doped MoS₂ with the optimal ratio is four times larger than that of bare MoS₂. Further PL spectra fittings show that the PL spectra of monolayer MoS₂ after V doping are dominated by the exciton peak, and the ratio of trion to total intensity in V-doped samples is decreased with increasing doping concentration, indicating that V doping as a p-type dopant makes exciton recombination prior to the negatively charged trion recombination. A similar decreased trion ratio in gate-dependent PL from –30 to 30 V further indicates the p-doping effect of V doping. Furthermore, the important role of V doping in PL intensity is further validated by comparing a slightly enhanced PL intensity through applying gate voltage with the largely enhanced PL intensity through V doping. Additionally, based on low-temperature PL spectra fitting using the Varshni equation, the optical band gap of monolayer MoS₂ changes from 1.920 to 1.847 eV after V doping, which could be attributed to the doping effects acting on electron–hole interactions in the V-doped samples. Moreover, on the basis of $I_{\text{ds}}-V_{\text{g}}$ curves of the as-fabricated field-effect transistors (FETs), the threshold voltage (V_{th}) is shifted in the positive direction from –10 to 12 V with increasing doping concentration, which arises from p-type doping. Combined with the enhanced PL intensity of V-doped monolayer MoSe₂, the ability of substitutional V doping to tune the optical properties of 2D TMDs are further confirmed.

■ ASSOCIATED CONTENT

Supporting Information

The Supporting Information is available free of charge at <https://pubs.acs.org/doi/10.1021/acsnm.0c03083>.

Optical characterization of V-doped MoS₂ with different concentrations, XPS survey spectra, PL testing results based on different monolayers, FETs properties and temperature-dependent PL spectra of as-prepared samples, and the related testing results of V-doped MoSe₂ (PDF)

■ AUTHOR INFORMATION

Corresponding Authors

Lifeng Wang – Institute for Frontier Materials, Deakin University, Victoria 3216, Australia; Email: lifeng.wang@deakin.edu.au

Yupeng Zhang – Institute of Microscale Optoelectronics, Shenzhen University, Shenzhen 518060, China; orcid.org/0000-0003-2351-5579; Email: ypzhang@szu.edu.cn

Yuerui Lu – Research School of Engineering, College of Engineering and Computer Science, The Australia National University, Canberra, Australian Capital Territory 2601, Australia; orcid.org/0000-0001-6131-3906; Email: yuerui.lu@anu.edu.au

Weiwei Lei – Institute for Frontier Materials, Deakin University, Victoria 3216, Australia; orcid.org/0000-0003-2698-299X; Email: Weiwei.Lei@deakin.edu.au

Authors

Jian Zhang – Institute of Microscale Optoelectronics, Shenzhen University, Shenzhen 518060, China; Research School of Engineering, College of Engineering and Computer Science, The Australia National University, Canberra, Australian Capital Territory 2601, Australia; orcid.org/0000-0002-0454-6751

Yi Zhu – Research School of Engineering, College of Engineering and Computer Science, The Australia National University, Canberra, Australian Capital Territory 2601, Australia

Mike Tebyetekerwa – Research School of Engineering, College of Engineering and Computer Science, The Australia National University, Canberra, Australian Capital Territory 2601, Australia; orcid.org/0000-0002-4243-6043

Delong Li – Institute of Microscale Optoelectronics, Shenzhen University, Shenzhen 518060, China

Dan Liu – Institute for Frontier Materials, Deakin University, Victoria 3216, Australia

Complete contact information is available at: <https://pubs.acs.org/10.1021/acsnm.0c03083>

Notes

The authors declare no competing financial interest.

■ ACKNOWLEDGMENTS

The authors acknowledge ACT node of the Australian National Fabrication Facility (ANFF). The authors acknowledge the Australian Research Council Discovery Program (DP190103290) and Nation Natural Science Foundation of China (51802104).

■ REFERENCES

- (1) Yue, Y.; Chen, J.; Zhang, Y.; Ding, S.; Zhao, F.; Wang, Y.; Zhang, D.; Li, R.; Dong, H.; Hu, W.; Feng, Y.; Feng, W. Two-Dimensional High-Quality Monolayered Triangular WS₂ Flakes for Field-Effect Transistors. *ACS Appl. Mater. Interfaces* **2018**, *10*, 22435–22444.
- (2) Gao, F.; Gong, Y.; Titze, M.; Almeida, R.; Ajayan, P. M.; Li, H. Valley trion dynamics in monolayer MoSe₂. *Phys. Rev. B: Condens. Matter Mater. Phys.* **2016**, *94*, 245413.
- (3) Tebyetekerwa, M.; Cheng, Y.; Zhang, J.; Li, W.; Li, H.; Neupane, G. P.; Wang, B.; Truong, T. N.; Xiao, C.; Al-Jassim, M.; Yin, Z.; Lu, Y.; Macdonald, D.; Nguyen, H. T. Emission Control from Transition Metal Dichalcogenide Monolayers by Aggregation-Induced Molecular Rotors. *ACS Nano* **2020**, *14*, 7444–7453.

- (4) Tebyetekerwa, M.; Zhang, J.; Liang, K.; Duong, T.; Neupane, G. P.; Zhang, L.; Liu, B.; Truong, T. N.; Basnet, R.; Qiao, X.; Yin, Z.; Lu, Y.; Macdonald, D.; Nguyen, H. T. Quantifying Quasi-Fermi Level Splitting and Mapping its Heterogeneity in Atomically Thin Transition Metal Dichalcogenides. *Adv. Mater.* **2019**, *31*, 1900522.

- (5) Eda, G.; Yamaguchi, H.; Voiry, D.; Fujita, T.; Chen, M.; Chhowalla, M. Photoluminescence from Chemically Exfoliated MoS₂. *Nano Lett.* **2011**, *11*, 5111–5116.

- (6) Duan, H.; Guo, P.; Wang, C.; Tan, H.; Hu, W.; Yan, W.; Ma, C.; Cai, L.; Song, L.; Zhang, W.; Sun, Z.; Wang, L.; Zhao, W.; Yin, Y.; Li, X.; Wei, S. Beating the Exclusion Rule against the Coexistence of Robust Luminescence and Ferromagnetism in Chalcogenide Monolayers. *Nat. Commun.* **2019**, *10*, 1584.

- (7) Zhang, X.; Nan, H.; Xiao, S.; Wan, X.; Ni, Z.; Gu, X.; Ostrikov, K. Shape-Uniform, High-Quality Monolayered MoS₂ Crystals for Gate-Tunable Photoluminescence. *ACS Appl. Mater. Interfaces* **2017**, *9*, 42121–42130.

- (8) Cadiz, F.; et al. Well Separated Trion and Neutral Excitons on Supercid Treated MoS₂ monolayers. *Appl. Phys. Lett.* **2016**, *108*, 251106.

- (9) Han, H. V.; Lu, A. Y.; Lu, L. S.; Huang, J. K.; Li, H.; Hsu, C. L.; Lin, Y. C.; Chiu, M. H.; Suenaga, K.; Chu, C. W.; Kuo, H. C.; Chang, W. H.; Li, L. J.; Shi, Y. Photoluminescence Enhancement and Structure Repairing of Monolayer MoSe₂ by Hydrohalic Acid Treatment. *ACS Nano* **2016**, *10*, 1454–1461.

- (10) Oh, H. M.; Han, G. H.; Kim, H.; Bae, J. J.; Jeong, M. S.; Lee, Y. H. Photochemical Reaction in Monolayer MoS₂ via Correlated Photoluminescence, Raman Spectroscopy, and Atomic Force Microscopy. *ACS Nano* **2016**, *10*, 5230–5236.

- (11) Qin, C.; Gao, Y.; Zhang, L.; Liang, X.; He, W.; Zhang, G.; Chen, R.; Hu, J.; Xiao, L.; Jia, S. Flexible Engineering of Light Emission in Monolayer MoS₂ via Direct Laser Writing for Multimode Optical Recording. *AIP Adv.* **2020**, *10*, 045230.

- (12) Qin, C.; Liang, X.; Han, S.; Zhang, G.; Chen, R.; Hu, J.; Xiao, L.; Jia, S. Giant Enhancement of Photoluminescence Emission in Monolayer WS₂ by Femtosecond Laser Irradiation. *Front. Phys.* **2021**, *16*, 12501.

- (13) Sim, D. M.; et al. Controlled Doping of Vacancy-Containing Few-Layer MoS₂ via Highly Stable Thiol-Based Molecular Chemisorption. *ACS Nano* **2015**, *9*, 12115–12123.

- (14) Mouri, S.; Miyauchi, Y.; Matsuda, K. Tunable Photoluminescence of Monolayer MoS₂ via Chemical Doping. *Nano Lett.* **2013**, *13*, 5944–5948.

- (15) Fang, H.; Tosun, M.; Seol, G.; Chang, T. C.; Takei, K.; Guo, J.; Javey, A. Degenerate n-Doping of Few-Layer Transition Metal Dichalcogenides by Potassium. *Nano Lett.* **2013**, *13*, 1991–1995.

- (16) Kiriya, D.; Tosun, M.; Zhao, P.; Kang, J. S.; Javey, A. Air-Stable Surface Charge Transfer Doping of MoS₂ by Benzyl Viologen. *J. Am. Chem. Soc.* **2014**, *136*, 7853–7856.

- (17) Lin, J. D.; Han, C.; Wang, F.; Wang, R.; Xiang, D.; Qin, S.; Zhang, X.; Wang, L.; Zhang, H.; Wee, A.; Chen, W. Electron-Doping-Enhanced Trion Formation in Monolayer Molybdenum Disulfide Functionalized with Cesium Carbonate. *ACS Nano* **2014**, *8*, 5323–5329.

- (18) Yang, L.; Majumdar, K.; Liu, H.; Du, Y.; Wu, H.; Hatzistergos, M.; Hung, P. Y.; Tieckelmann, R.; Tsai, W.; Hobbs, C.; Ye, P. D. Chloride Molecular Doping Technique on 2D Materials: WS₂ and MoS₂. *Nano Lett.* **2014**, *14*, 6275–6280.

- (19) Zhu, J.; Zhang, H.; Tong, Y.; Zhao, L.; Zhang, Y.; Qiu, Y.; Lin, X. First-Principles Investigations of Metal (V, Nb, Ta)-Doped Monolayer MoS₂: Structural Stability, Electronic Properties and Adsorption of Gas Molecules. *Appl. Surf. Sci.* **2017**, *419*, 522–530.

- (20) Williamson, I.; Li, S.; Correa Hernandez, A.; Lawson, M.; Chen, Y.; Li, L. Structural, Electrical, Phonon, and Optical Properties of Ti- and V-Doped Two-Dimensional MoS₂. *Chem. Phys. Lett.* **2017**, *674*, 157–163.

- (21) Wang, Y.; Tseng, L.-T.; Murmu, P. P.; Bao, N.; Kennedy, J.; Ionesc, M.; Ding, J.; Suzuki, K.; Li, S.; Yi, J. Defects Engineering

Induced Room Temperature Ferromagnetism in Transition Metal Doped MoS₂. *Mater. Des.* **2017**, *121*, 77–84.

(22) Fan, X. L.; An, Y. R.; Guo, W. J. Ferromagnetism in Transitional Metal-Doped MoS₂ Monolayer. *Nanoscale Res. Lett.* **2016**, *11*, 154.

(23) Gao, J.; Kim, Y. D.; Liang, L.; Idrobo, J. C.; Chow, P.; Tan, J.; Li, B.; Li, L.; Sumpter, B. G.; Lu, T. M.; Meunier, V.; Hone, J.; Koratkar, N. Transition-Metal Substitution Doping in Synthetic Atomically Thin Semiconductors. *Adv. Mater.* **2016**, *28*, 9735–9743.

(24) Kochat, V.; Apte, A.; Hachtel, J. A.; Kumazoe, H.; Krishnamoorthy, A.; Susarla, S.; Idrobo, J. C.; Shimojo, F.; Vashishta, P.; Kalia, R.; Nakano, A.; Tiwary, C. S.; Ajayan, P. M. Re Doping in 2D Transition Metal Dichalcogenides as a New Route to Tailor Structural Phases and Induced Magnetism. *Adv. Mater.* **2017**, *29*, 1703754.

(25) Suh, J.; Park, T. E.; Lin, D. Y.; Fu, D.; Park, J.; Jung, H. J.; Chen, Y.; Ko, C.; Jang, C.; Sun, Y.; Sinclair, R.; Chang, J.; Tongay, S.; Wu, J. Doping against the Native Propensity of MoS₂: Degenerate Hole Doping by Cation Substitution. *Nano Lett.* **2014**, *14*, 6976–6982.

(26) Zhang, K.; Feng, S.; Wang, J.; Azcatl, A.; Lu, N.; Addou, R.; Wang, N.; Zhou, C.; Lerach, J.; Bojan, V.; Kim, M. J.; Chen, L. Q.; Wallace, R. M.; Terrones, M.; Zhu, J.; Robinson, J. A. Manganese Doping of Monolayer MoS₂: The Substrate Is Critical. *Nano Lett.* **2015**, *15*, 6586–6591.

(27) Zhang, K.; Bersch, B. M.; Joshi, J.; Addou, R.; Cormier, C. R.; Zhang, C.; Xu, K.; Briggs, N. C.; Wang, K.; Subramanian, S.; Cho, K.; Fullerton-Shirey, S.; Wallace, R. M.; Vora, P. M.; Robinson, J. A. Tuning the Electronic and Photonic Properties of Monolayer MoS₂ via In Situ Rhenium Substitutional Doping. *Adv. Funct. Mater.* **2018**, *28*, 1706950.

(28) Zhang, J.; Wang, B.; Tebyetekerwa, M.; Zhu, Y.; Liu, B.; Nguyen, H. T.; Tian, S.; Zhang, Y.; Lu, Y. Aluminium and Zinc co-Doped CuInS₂ QDs for Enhanced Trion Modulation in Monolayer WS₂ toward Improved Electrical Properties. *J. Mater. Chem. C* **2019**, *7*, 15074–15081.

(29) Zhang, W.; Huang, J. K.; Chen, C. H.; Chang, Y. H.; Cheng, Y. J.; Li, L. J. High-Gain Phototransistors Based on a CVD MoS₂ Monolayer. *Adv. Mater.* **2013**, *25*, 3456–3461.

(30) Chakraborty, B.; Bera, A.; Muthu, D. V. S.; Bhowmick, S.; Waghmare, U. V.; Sood, A. K. Symmetry-Dependent Phonon Renormalization in Monolayer MoS₂ Transistor. *Phys. Rev. B: Condens. Matter Mater. Phys.* **2012**, *85*, 161403.

(31) Zhang, S.; Hill, H. M.; Moudgil, K.; Richter, C. A.; Hight Walker, A. R.; Barlow, S.; Marder, S. R.; Hacker, C. A.; Pookpanratana, S. J. Controllable, Wide-Ranging n-Doping and p-Doping of Monolayer Group 6 Transition-Metal Disulfides and Diselenides. *Adv. Mater.* **2018**, *30*, No. e1802991.

(32) Xu, R.; Zhang, S.; Wang, F.; Yang, J.; Wang, Z.; Pei, J.; Myint, Y. W.; Xing, B.; Yu, Z.; Fu, L.; Qin, Q.; Lu, Y. Extraordinarily Bound Quasi-One-Dimensional Trions in Two-Dimensional Phosphorene Atomic Semiconductors. *ACS Nano* **2016**, *10*, 2046–2053.

(33) Xu, R.; Yang, J.; Zhu, Y.; Yan, H.; Pei, J.; Myint, Y. W.; Zhang, S.; Lu, Y. Layer-Dependent Surface Potential of Phosphorene and Anisotropic/Layer-Dependent Charge Transfer in Phosphorene-Gold Hybrid Systems. *Nanoscale* **2016**, *8*, 129–135.

(34) Yang, J.; Xu, R.; Pei, J.; Myint, Y. W.; Wang, F.; Wang, Z.; Zhang, S.; Yu, Z.; Lu, Y. Optical Tuning of Exciton and Trion Emissions in Monolayer Phosphorene. *Light: Sci. Appl.* **2015**, *4*, No. e312.

(35) Zhang, T.; Fujisawa, K.; Zhang, F.; Liu, M.; Lucking, M. C.; Gontijo, R. N.; Lei, Y.; Liu, H.; Crust, K.; Granzier-Nakajima, T.; Terrones, H.; Elias, A. L.; Terrones, M. Universal In Situ Substitutional Doping of Transition Metal Dichalcogenides by Liquid-Phase Precursor-Assisted Synthesis. *ACS Nano* **2020**, *14*, 4326–4335.

(36) Dolui, K.; Rungger, I.; Das Pemmaraju, C.; Sanvito, S. Possible Doping Strategies for MoS₂ Monolayers: An ab initio study. *Phys. Rev. B: Condens. Matter Mater. Phys.* **2013**, *88*, 075420.

(37) Pham, V. P.; Yeom, G. Y. Recent Advances in Doping of Molybdenum Disulfide: Industrial Applications and Future Prospects. *Adv. Mater.* **2016**, *28*, 9024–9059.

(38) Ross, J. S.; Wu, S.; Yu, H.; Ghimire, N. J.; Jones, A. M.; Aivazian, G.; Yan, J.; Mandrus, D. G.; Xiao, D.; Yao, W.; Xu, X. Electrical Control of Neutral and Charged Excitons in a Monolayer Semiconductor. *Nat. Commun.* **2013**, *4*, 1474.

(39) Lin, Y.; Ling, X.; Yu, L.; Huang, S.; Hsu, A. L.; Lee, Y. H.; Kong, J.; Dresselhaus, M. S.; Palacios, T. Dielectric Screening of Excitons and Trions in Single-layer MoS₂. *Nano Lett.* **2014**, *14*, 5569–5576.

(40) Kioseoglou, G.; Hanbicki, A. T.; Currie, M.; Friedman, A. L.; Gunlycke, D.; Jonker, B. T. Valley Polarization and Intervalley Scattering in Monolayer MoS₂. *Appl. Phys. Lett.* **2012**, *101*, 221907.

(41) Korn, T.; Heydrich, S.; Hirmer, M.; Schmutzler, J.; Schuller, C. Low-Temperature Photocarrier Dynamics in Monolayer MoS₂. *Appl. Phys. Lett.* **2011**, *99*, 102109.

(42) Ugeda, M. M.; Bradley, A. J.; Shi, S.-F.; da Jornada, F. H.; Zhang, Y.; Qiu, D. Y.; Ruan, W.; Mo, S.-K.; Hussain, Z.; Shen, Z.-X.; Wang, F.; Louie, S. G.; Crommie, M. F. Giant Bandgap Renormalization and Excitonic Effects in A Monolayer Transition Metal Dichalcogenide Semiconductor. *Nat. Mater.* **2014**, *13*, 1091–1095.

(43) Peelaers, H.; Van de Walle, C. G. Effects of Strain on Band Structure and Effective Masses in MoS₂. *Phys. Rev. B: Condens. Matter Mater. Phys.* **2012**, *86*, 241401.

(44) Borghardt, S.; Tu, J.; Winkler, F.; Schubert, J.; Zander, W.; Leosson, K.; Kardynal, B. E. Engineering of Optical and Electronic Band Gaps in Transition Metal Dichalcogenide Monolayers through External Dielectric Screening. *Phys. Rev. Mater.* **2017**, *1*, 054001.

(45) Su, S.-H.; Hsu, Y.-T.; Chang, Y.-H.; Chiu, M.-H.; Hsu, C.-L.; Hsu, W.-T.; Chang, W.-H.; He, J.-H.; Li, L.-J. Band Gap-Tunable Molybdenum Sulfide Selenide Monolayer Alloy. *Small* **2014**, *10*, 2589–2594.